


RESEARCH ARTICLE

Open Access



# Robotic 3D printed lunar bionic architecture based on lunar regolith selective laser sintering technology

Philip F. Yuan<sup>1\*</sup> , Xinjie Zhou<sup>1</sup>, Hao Wu<sup>1</sup>, Liming Zhang<sup>1</sup>, Lijie Guo<sup>2</sup>, Yun Shi<sup>2</sup>, Zhe Lin<sup>3</sup>, Jinyu Bai<sup>3</sup>, Youhai Yu<sup>4\*</sup> and Shanglu Yang<sup>3\*</sup>

## Abstract

The lunar base is not only an experimental station for extraterrestrial space exploration but also a dwelling for humans performing this exploration. Building a lunar base presents numerous obstacles and requires environmental perception, feedback design, and construction methods. An integrated fabrication process that incorporates design, 3D printing workflow, and construction details to build a bionic, reconfigurable and high-performance lunar base prototype is presented in this paper. The research comprises the study of the lunar regolith 3D printing mechanism, the real-time control of powder laying and compaction procedure, and the development of a 3D printing tool end system. In this paper, many scientific questions regarding in situ fabrication on the lunar surface are raised and addressed with the proposal of a progressive optimization design method, the molding principle, and gradation strategy of lunar soil-polyaryletherketone (PAEK) hybrid powder, and the principle of dual-light field 3D laser printing. The feasibility of the technical strategy proposed in this paper is verified by the presented empirical samples.

**Keywords:** Lunar architecture design, Lunar base construction, In situ fabrication, 3D laser printing, Printable lunar regolith, Extraterrestrial habitation

## 1 Introduction

Human exploration of the moon began in the 1960s. Since the beginning of the twenty-first century, different nations have landed on the moon and conducted lunar exploration research. In 2005, NASA proposed the Centennial Challenges (Baum, 2006), which included 3D printing of space stations and space robots, all of which were related to lunar surface construction. In 2019, NASA proposed the Artemis program (Evan & Graham, 2020), which aimed to complete a lunar base as early as

2028. Countries such as Russia, Europe, Japan, South Korea, and India have also participated in an international cooperation research on lunar exploration. For example, the EU and Russia plan to jointly launch the Luna27 lunar south pole probe after 2022 (King et al., 2020). In 2019, Li Chunlai, director of the National Astronomical Observatory of the Chinese Academy of Sciences, published an article in Science proposing to carry out an 'exploration, construction, and operation' mission plan that aimed to be completed before 2030 (Li et al., 2019a). According to the China National Space Agency's lunar exploration mission plan, aside from scientific exploration, the "Chang'e 8" aimed to conduct field research for in situ construction with lunar regolith.

The lunar base can serve as an experimental station for extraterrestrial space exploration, as well as a detection outpost for extraterrestrial human settlements. The construction of the lunar base encompasses four stages:

\*Correspondence: philipyuan007@tongji.edu.cn; yuyouhai@dhu.edu.cn; yangshanglu@siom.ac.cn

<sup>1</sup> College of Architecture and Urban Planning, Tongji University, Shanghai, China

<sup>3</sup> Shanghai Institute of Optics and Fine Mechanics, Chinese Academy of Sciences, Shanghai, China

<sup>4</sup> Center for Advanced Low-dimension Materials, Donghua University, Shanghai, China

Full list of author information is available at the end of the article

preliminary preparation, infrastructure construction, base construction, and post-operation. The research process of these four stages requires an integrated multidisciplinary collaboration between different expertise. Architectural and civil engineering research plays a crucial role in lunar base construction processes, such as site selection, base planning, space design, and base construction.

The complex and multidimensional characteristics of the lunar environment (Vaniman et al., 1991) provided numerous complex design requirements for lunar structures. Since the lunar surface is in a vacuum environment with no atmosphere, and a high fraction of extremely fine particles in the lunar regolith has high penetrability and electrostatic viscosity, high airtightness is required for human settlement on the lunar surface. In addition, the structure must be impact-resistant due to the possibility of micrometeorite bombardment. On the lunar surface, the dose of cosmic radiation particles is quite high and can cause damage to the human body and architectural structures, so the lunar base must be able to protect against space radiation. At the same time, because of the lack of atmosphere, the surface of the lunar base exposed to solar radiation will produce a very large temperature difference between day and night, so the construction of the lunar base should consider the temperature effect.

Since the 1980s, scientists from around the world have begun developing the idea of constructing a lunar base. Three key development phases are as follows. In the first phase, pre-integrated tanks are created on Earth and transported to the lunar surface for splicing. In the second phase, prefabricated inflatable devices are developed on Earth and deployed on the moon. Finally, in the third phase, the inflated membrane structure are used as a basic structure, and a layer of radiation-resistant and high-temperature-resistant cladding are built with lunar regolith in situ fabrication technology (Howe & Sherwood, 2009).

The first phase does not necessitate a complex basis for the utilization of lunar resources and does not place excessive demands on the lunar terrain environment. It uses a modular design, and its morphological structure is tightly integrated with its internal functions. Examples include the LS3 lunar outpost (Kennedy & Toups, 2008) and the Hubbert lunar base conceptual scheme (Dudley-Rowley et al., 2005).

The second phase has the following characteristics: it is less limited by the size and capacity of the launch vehicle and can typically achieve a greater construction volume on the lunar surface. These lunar-deployable structures are constructed on Earth and fully commissioned to allow automatic or semiautomatic assembly and deployment when rocketed to the lunar surface. The

inflated-torus concept (Howe & Sherwood, 2009) and the transformable robotic infrastructure-generating object network (TRIGON) (Howe & Gibson, 2006) are two representative examples.

The third phase uses a construction technology that utilizes lunar in situ resources as the primary building material. Through resource mining and processing, the lunar regolith is converted into additive manufacturing (AM) raw materials. This in situ construction technology relies on a variety of technologies, including satellite detection of lunar soil, lunar soil mining, lunar soil optimization, base site selection, and lunar soil printing. Examples include the Sinterhub scheme (Tomas et al., 2012) and the Chinese Super Mason scheme (Zhou et al., 2019).

## 2 State-of-the-art Lunar Base construction exploration

### 2.1 Lunar base design based on the in situ construction method

The in situ construction method, which incorporates partially preassembled Earth components, is an effective and sustainable solution for reducing the weight of rocket launches while achieving large-scale lunar base construction. In this paper, three projects that adopted this construction method were selected: the Sinterhub scheme proposed by NASA's Marshall Space Flight Center (Tomas et al., 2012); the lunar outpost design concept proposed by ESA and Foster (Foster + Partners, 2012); and the "China Super Mason" scheme proposed by the Huazhong University of Science and Technology (Zhou et al., 2019). Based on a set of evaluation indicators constructed by the author, the characteristics of these three projects were evaluated, as shown in Table 1.

Both Sinterhub and Lunar Habitation use a microwave sintering process that does not require the carrying of earth materials but places high demands on the energy supply and low printing accuracy. Sinterhub requires a larger robot to create large spaces, while Lunar Habitation does not. The robot can crawl on the inflatable membrane to build; however, this requires a higher structural strength of the inflatable membrane. The Chinese Super Mason uses a high-temperature autoclave to manufacture lunar bricks, which requires 10% of Earth materials. After the lunar bricks are formed, the structure is constructed by robotic masonry. However, this method requires a large amount of energy supply and requires high robot positioning accuracy, and the size of the building that can be built is limited by the size of the robot.

The above analysis demonstrates that the construction method of deploying the inflatable membrane and then covering it with lunar soil is capable of constructing a large-scale lunar base space. Since 3D printing

**Table 1** Comparison of the project features

Criterion	Sinterhub (NASA)		Lunar Habitation (ESA & Foster + Partners)		Chinese Super Mason (HZUST)	
	Marks	Features	Marks	Features	Marks	Features
In situ construction process	4/5	With selective microwave sintering technology, the microwaves' penetrating power creates a dense structure.	4/5	With selective microwave sintering technology, the microwave penetrating power creates a dense structure.	4/5	High-temperature autoclave forms a compact and dense structure.
Energy consumption per mass structure unit	3/5	600 kWh/m <sup>3</sup> , the microwave sintering processes energy consumption is high but lower than high-temperature autoclave.	3/5	600 kWh/m <sup>3</sup> , the microwave sintering processes energy consumption is high but lower than high-temperature autoclave.	1/5	Autoclaved for 8 hours at 195°C and 1.4MPa, each autoclave has a volume of approximately 10 cm <sup>3</sup> .
Lunar soil to Earth material ratio per unit mass of hybrid powder	5/5	No earth material required	5/5	No earth material required	3/5	Unit mass of mixed material contains 10% Ca (OH) <sub>2</sub>
Construction methods and challenges	3/5	Expand the inflatable membrane and cover it with lunar soil for solar sintering	3/5	Expand the inflatable membrane and cover it with lunar soil for solar sintering	1/5	The robotic arm autoclaves and assembles the lunar soil bricks. During construction, the problem of precise positioning needs to be addressed.
Size of the formed space	4/5	Depending on the robot size, larger robots form larger spaces	4/5	Microwave sintering robots can climb onto the inflatable membrane, enable to form a bigger space.	2/5	Space created is limited due to the size of the masonry robot.
Systems requiring prelaunch	2/5	Inflatable membrane, solar-powered microwave sintering robot	4/5	Inflatable membrane, solar-powered microwave sintering robot	3/5	Inflatable membrane, masonry robot, high-temperature autoclave forming equipment
Energy acquisition method	3/5	Solar Energy	3/5	Solar Energy	4/5	Nuclear and solar energy
Sum	24/35		26/35		18/35	

technology is adaptable to diverse site conditions, it has advantages for this in situ construction scheme. However, it is necessary to reduce the amount of energy to be supplied for the purpose of improving the accuracy. Based on this result, a 3D laser-printing design and construction method with a hybrid powder of lunar soil and polyaryletherketone (PAEK), which requires less energy consumption and is more accurate, is proposed in this paper.

### 2.2 State-of-the-art lunar soil in situ 3D printing technology

In situ resource utilization (ISRU) refers to the construction technology that utilizes lunar in situ resources as the primary building materials (Anand et al., 2012). Regolith lunar soil is turned into raw materials for additive manufacturing (AM) primarily by mining and processing. Due to the exorbitant expense of transporting rockets and the rarity and scarcity of lunar soil on Earth, all in situ construction tests of lunar soil were conducted using regolith simulant. The replicated lunar soil is a geochemical copy of the lunar sample, with identical mineral and chemical composition, grain size, mechanical strength, porosity, density, and electrical properties (He et al., 2013; McKay et al., 1993). As the first institution of higher education in China to conduct research on regolith simulants, Tongji University has produced Tongji-1 (TJ-1 for short) and conducted quantitative analytical studies on its physical bearing qualities and microstructure (Jiang et al., 2012).

Based on domestic and international research, there are five primary types of additive manufacturing processes for lunar regolith based on regolith simulant.

- Material extrusion/jetting: Premixed pastes made of regolith simulant and liquid binders are used as the printing material to build 3D objects layer by layer (Travitzky et al., 2014; Khoshnevis et al., 2005). Example methods are contour crafting technology (Lin et al., 1989; Fiske & Edmunson, 2017; Oh et al., 2020; Lee et al., 2015), binder-jetting technology (Ceccanti et al., 2010; Cesaretti et al., 2014), and ink-jetting technology (Jakus et al., 2017; Taylor et al., 2018).
- Powder bed fusion (PBF): Through powder laying, selective sintering of powder layers with energy beams can achieve layer-by-layer desired 3D printing outcomes (Chen et al., 2019). There are several variants of this technology: selective solar light sintering (SSLS) (Li et al., 2018; Magoffin & Garvey, 1990; Nakamura et al., 2008; Hintze et al., 2009), selective laser sintering/melting (SLS/SLM) (Goulas et al., 2017; Goulas et al., 2019; Fateri et al., 2015), and selective microwave sintering (SMWS) (Khoshnevis and Zhang, 2015).
- Laser Engineered Net Shaping (LENS): Premixed powder is melted by an energy beam under the protection of inert gas, and the molten powder slurry is printed to build a 3D object (Balla et al., 2012; Mueller et al., 2014a, b).
- Selective Microwave Sintering (SMWS): Regolith is heated by the penetration of microwaves and sintered into shape (Taylor & Meek, 2005).
- Stereolithography/Digital Light Processing (SLA/DLP): Layer-by-layer application of a slurry composed of lunar soil and an organic binder and UV

**Table 2** Comparison of additive manufacturing processes

Regolith printing techniques	Material extrusion/jetting	Powder bed fusion (PBF) (Solar light sintering/laser sintering)	Laser engineered net shaping (Lens)	Selective microwave sintering	Stereolithography/Digital light processing
<b>Energy consumption</b>	20-50 kWh/m <sup>3</sup>	20-50 kWh/m <sup>3</sup>	2300 kWh/m <sup>3</sup>	500 kWh/m <sup>3</sup>	50 kWh/m <sup>3</sup>
<b>Consumables (per 100 kg)</b>	25-35 kg binder Inert gas for paste/powder distribution	Direct sintering or adding a small amount of binder	Inert gas for paste/powder distribution	Direct sintering or adding a small amount of binder	15-30 kg photopolymer
<b>Printing speed</b>	6-12 m/min	3 m/min	1.2 m/min	Nil	Nil
<b>Printing accuracy</b>	0.5-3.2 mm	0.2 mm	1.65 mm	10-20 mm	0.02 mm
<b>Compressive ability</b>	20-50 MPa	22-35 MPa	Nil	Nil	Nil
<b>Auxiliary conditions</b>	Inert gas required	/	Inert gas required	/	/
<b>Features</b>	Low energy consumption More consumables Inert gas required Fast printing High printing accuracy	Low energy consumption Lesser consumables Fast and high printing accuracy	Very high energy consumption Inert gas required Slow printing Low printing accuracy	Very high energy consumption Inert gas required Slow printing Low printing accuracy	Low energy consumption More consumables High printing accuracy

laser beam photopolymerization of the slurry (Travitzky et al., 2014; Liu et al., 2019).

We compare these five types in Table 2. This research focuses on studying the powder bed fusion process, specifically the selective laser sintering (SLS) technique, which can produce gridded spatial structure printing, after an in-depth evaluation of the aforementioned approaches on aspects of coupling, operability, and process complexity. Polyaryletherketone is a common substance in the aircraft industry (Rinaldi et al., 2021). By recycling spacecraft, parachutes, and landing airbags, polyaryletherketone can be utilized to manufacture printing materials (Li & Englund, 2017). Polyaryletherketone is an ideal regolith sintering material additive because it can lower the sintering temperature and save considerable energy while improving the printing efficiency. Low energy consumption, fewer consumables, fast printing speed, excellent precision, and high-pressure resistance are all advantages of the mixed powder of polyaryletherketone and regolith.

### 3 Architectural conceptual design for lunar habitats

The shells are in a buoyant seawater environment similar to the low gravity environment of the lunar surface, and their morphology contains many geometric features adapted to this environment (Gailunas, 2015). At the same time, the shell structure protects its internal structure from predators and other potentially dangerous threats (Knippers et al., 2019). Developing shell form became an important focus for modern architectural design (especially thin-shelled buildings) to imitate, such as the famous Sydney Opera House (Rey-Rey, 2022). The unique mother-of-pearl structure inside the shell can provide a prototype for the design of lightweight and high-strength structures (Sun and Bhushan, 2012). Based on this, we put forward our concept of Moon-base buildings (Fig. 1) based on the mollusk shell structure, and the required research steps include the following steps.

1. Challenging environmental conditions such as vacuum environments, microgravity, extreme heat and cold, and powerful radiation are studied and understood; a virtual 3D model (Yuan et al., 2021) is constructed, and building load simulation tests are executed under maximum bearing capacity and normal bearing capacity; a performance parameter index system is constructed for evaluation purposes.
2. The geometric prototype of the lunar base skin is designed based on a microgravity state analysis and force simulation of marine shellfish; macroscopically, the optimal geometric configuration of the shell is

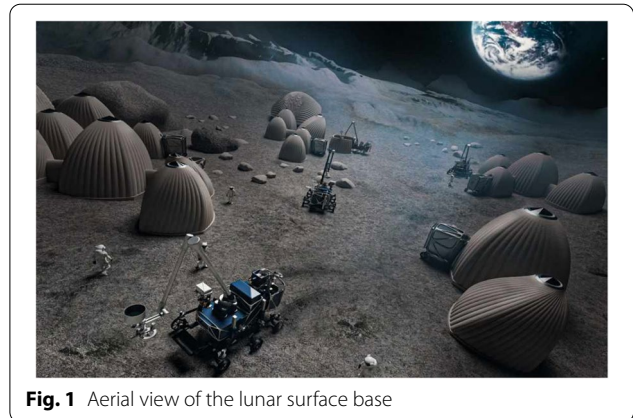


**Fig. 1** Aerial view of the lunar surface base

determined using mathematical geometric principles, a thrust network analysis method (Li et al., 2019a, 2019b), a dynamic simulation analysis, and a printability collaborative design; microscopically, BESO (Long et al., 2018) is used to improve the efficiency of material structures and achieve the multi-layer structure system of lightweight, low-material, and high-efficiency wall, based on a simulation analysis of the shell nacre structural layers.

3. On the basis of the FURobot robot simulation platform (Lu et al., 2020), the potential field approach (Hwang & Ahuja, 1992) and sampling-based motion planning (Lindemann & LaValle, 1992) are fully applied to achieve real-time obstacle avoidance of the end effector in a complicated environment. A large-scale lunar soil 3D printing integrated control system is researched and developed to achieve the full-process control of the integrated construction of the lunar surface.

#### 3.1 Design prototype for lunar gravity-adapted bionic structures

In this section, the design process of lunar gravity-adapted bionic structures is introduced in three main parts (Fig. 2). First, the basic environmental parameters of the Moon need to be determined; second, a bionic building geometry prototype needs to be constructed; and finally, a performance evaluation system needs to be constructed.

##### 3.1.1 Analysis of lunar surface characteristics

Analyzing the unique environmental properties of the lunar surface is crucial for the design of the lunar base and 3D printing processes. The lunar environment possesses extreme features, such as a vacuum atmosphere, microgravity, extreme high and low temperatures, and



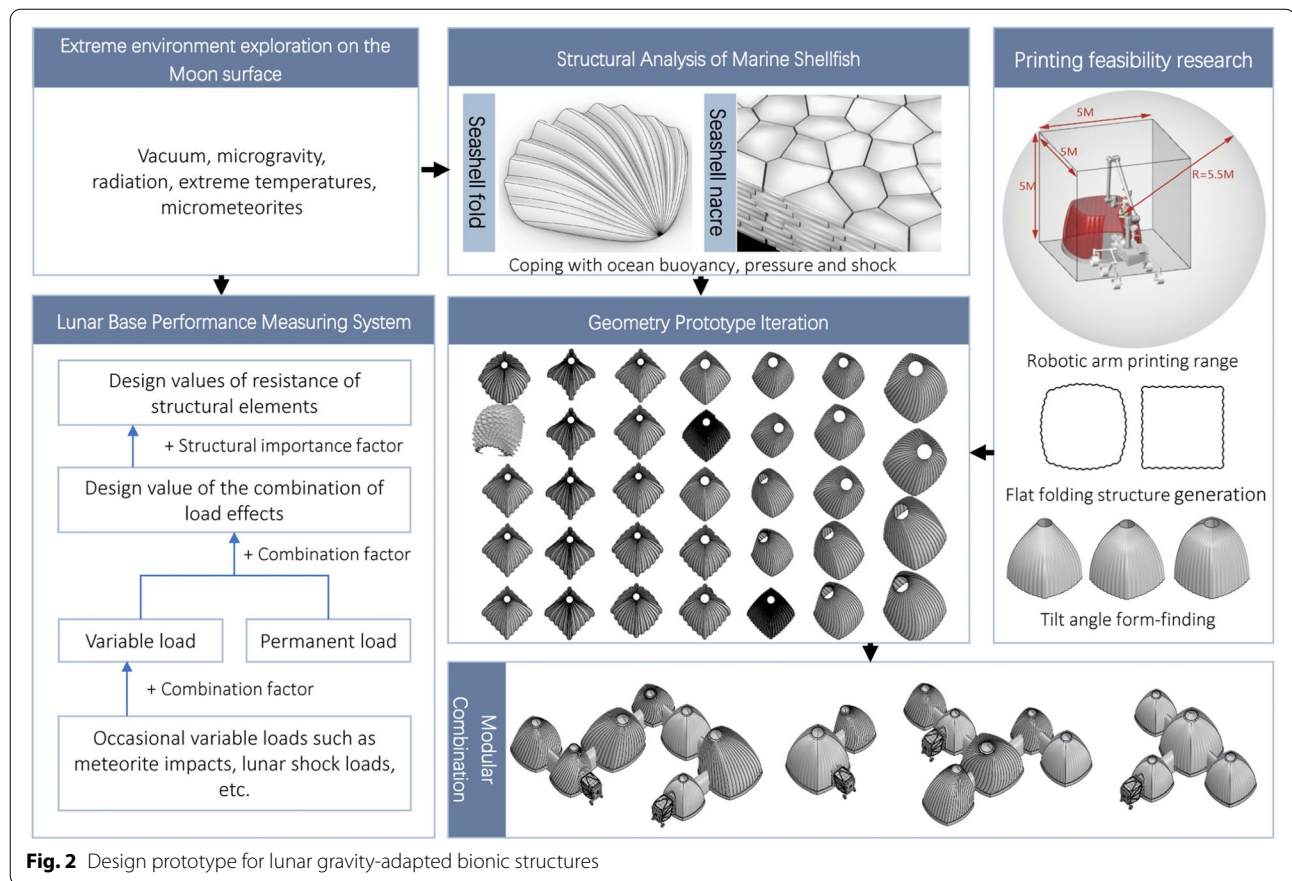


**Fig. 2** Design prototype for lunar gravity-adapted bionic structures

intense radiation (Vaniman et al., 1991). The gravitational acceleration of the lunar surface is approximately one-sixth that of Earth, or  $1.62\text{ m}\cdot\text{s}^{-2}$  (Vaniman et al., 1991); the radiation on the lunar surface consists of cosmic radiation, lunar radiation, and secondary radiation, with the average dose of Galactic Cosmic Radiation (GCR) on the surface of the Moon being equivalent to  $1369\text{ }\mu\text{Sv}/\text{day}$  (Zhang et al., 2020); the temperature difference between day and night on the lunar surface varies, ranging between  $95\text{ K}$ - $387\text{ K}$  at the equator, with a maximum rate of variation of  $150\text{ K}$  per hour (Williams et al., 2017); the average speed of micrometeorites is  $20\text{ km}/\text{s}$  (Allende et al., 2020); and the maximum magnitude of moonquakes is 5 (Goins et al., 1981).

### 3.1.2 Geometric prototype design of adaptive bionic structures

Based on the microgravity state study of marine shell structures, their compressive, tensile, and flexural characteristics were defined and simulated, and a parametric analysis framework for bionic structures was provided. Additionally, the inorganic bridging function of the shell nacre and its hardening mechanism were

we analyzed to design the geometric prototype of the biomimetic folding skin of the lunar architecture, taking the printability of the printing end effector into account. Moreover, the group combination mode of bionic space prototypes was studied to explore the reconfigurable combination mode of single space geometric prototypes.

#### 3.1.3 Developing a performance index for the lunar base

For the complicated lunar surface environmental loads borne by buildings on the lunar surface, the load combinations are carried out in accordance with the limit states of the bearing capacity and normal use. For the limit state of the bearing capacity, the fundamental combination or accidental combination of the load effect is utilized to compute the effect design value of the load combination. The formula is as follows:

$$\gamma_0 S_d \leq R_d$$

where:

$\gamma_0$  - the coefficient of structural importance of the lunar building, with reference to ordinary buildings, where the larger value is chosen.

$S_d$  - the design value of the combination of load effects.

$R_d$  - the design value of the resistance of the structural elements.

For the lunar surface microgravity environment and temperature effect, the variable load control effect design value is adopted. For the occasional variable load, such as meteorite impact and moonquake load, a combination of accidental load and variable load is adopted, and the most unfavorable effect design value is adopted.

The design value of the effect controlled by the variable load is calculated by the following equation.

$$S_d = \sum_{j=1}^m \gamma_{Gj} S_{Gjk} + \gamma_{Q1} \gamma_{L1} S_{Q1k} + \sum_{i=2}^n \gamma_{Qi} \gamma_{Li} \psi_{ci} S_{Qik}$$

where:

$\gamma_{Gj}$  - The subfactor for the j-th permanent load.

$\gamma_{Qi}$  - The subfactor of the i-th variable load, where  $\gamma_{Q1}$  is the subfactor of the dominant variable load  $Q_1$ .

$\gamma_{Li}$  - The adjustment factor for the i-th variable load considering the design service life, where  $\gamma_{L1}$  is the adjustment factor for the dominant variable load  $Q_1$  considering the design service life.

$S_{Gjk}$  - the value of the load effect calculated for the jth standard value of permanent load  $G_k$ , here mainly permanent loads such as microgravity on the moon surface and functional forces on the structure.

$S_{Qik}$  - The value of the load effect calculated by the standard value of the i-th variable load,  $Q_{ik}$ , where  $S_{Q1k}$  is the variable load that plays the most significant role among the various variable load effects.

$\psi_{ci}$  - The coefficient of the combined value of the i-th variable load  $Q_i$ .

$m$  - The number of permanent loads involved in the combination.

$n$  - The number of variable loads involved in the combination.

The design value of the effect used for the limit state calculation of the load carrying capacity is calculated according to the following formula:

$$S_d = \sum_{j=1}^m S_{Gjk} + S_{Ad} + \psi_{f1} S_{Q1k} + \sum_{i=2}^n \psi_{qi} S_{Qik}$$

The effect design value for the overall structural stability verification of the damaged lunar structure after suffering a chance event is calculated by the following equation.

$$S_d = \sum_{j=1}^m S_{Gjk} + \psi_{f1} S_{Q1k} + \sum_{i=2}^n \psi_{qi} S_{Qik}$$

where:

$S_{Ad}$  - The value of the load effect calculated by the standard value of the incidental load  $A_d$ .

$\psi_{f1}$  - The coefficient of the frequency value of the 1st variable load.

$\psi_{qi}$  - Quasi-permanent value factor for the i-th variable load.

### 3.2 Design approaches for a lightweight and high-performance lunar base

In this section, the design methodology of lightweight high-performance lunar base structures (Fig. 3) is presented in three main aspects. The first aspect is the establishment of lightweight lunar base building prototypes, the second is the optimization of macrostructure topology, and finally, the third is the optimization of wall microstructures.

#### 3.2.1 Lightweight lunar base architectural prototype

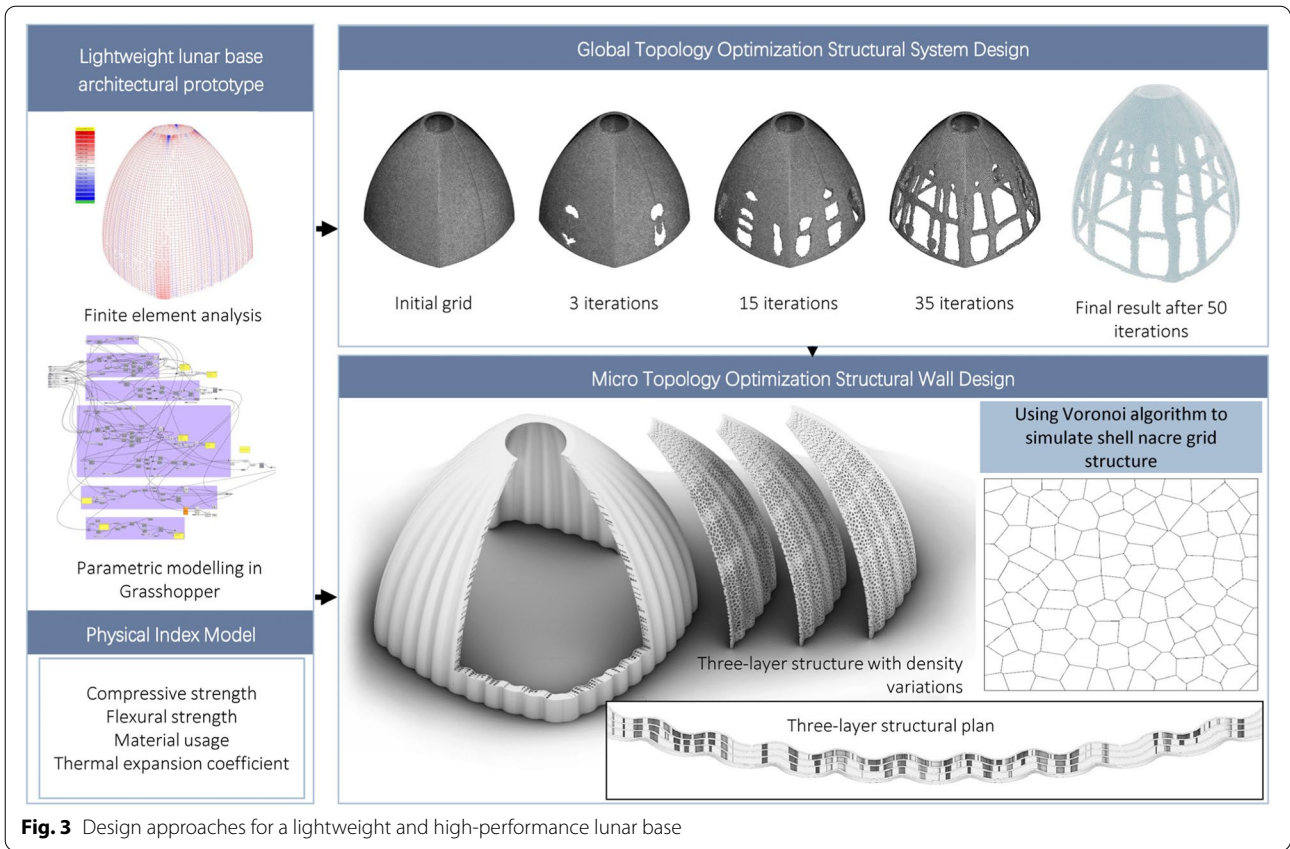
To reduce the transportation cost and if the maximum use rate of regolith is achieved, the lunar base should adopt a lightweight structural design that decreases the amount of materials while maintaining the structural efficiency. To achieve a high-performance lightweight shell structure, the finite element method is utilized for structural analysis, parametric modeling technology is used to realize rapid modification and iteration of the design, and the topology optimization algorithm is used to optimize the material distribution. A theoretical analysis framework that includes a virtual model of the lunar base with physical parameters should be constructed to test the number of materials used, compressive strength, flexural strength, coefficient of thermal expansion, etc.

#### 3.2.2 Global topology optimization structural system design

In this research, a set of lunar base building block design methods are proposed. These methods consist of plane geometry calculation, overall shape control, and structural performance optimization based on mathematical geometric principles, the thrust line grid analysis method (Avelino et al., 2021), and dynamic simulation analysis, in conjunction with BESO (Long et al., 2018). To determine the optimal geometric configuration of the shell, other factors, such as the shell slope, plane curve curvature, 3D printing head shape, and path planning and design, are considered.

#### 3.2.3 Micro-topology optimization for the development of anti-collision structural walls

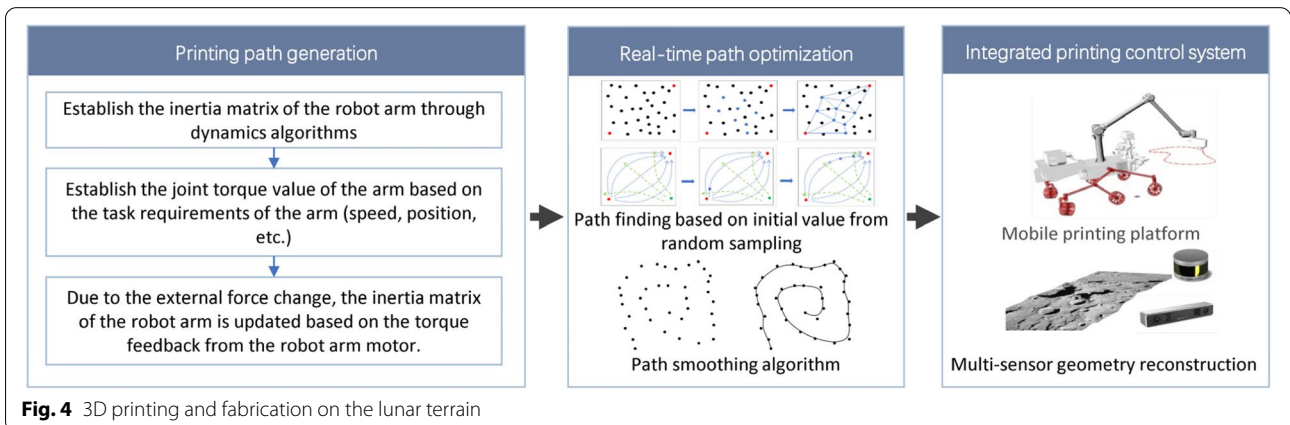
By utilizing a simulation analysis of the shell nacre structural layers, the hollow structure is used to optimize the



wall structure of the lunar base to achieve the lowest possible weight. The design method of a multilayer structure is adopted to enhance the impact resistance of the structure. Combined with the end effector, the printability analysis of the optimized lunar base wall is performed, and the analysis framework of the lunar base’s micro-topology optimization structure is formulated.

### 3.3 3D printing and fabrication on the lunar terrain

In this section, the method of 3D printing in the complex terrain environment of the Moon (Fig. 4) is described. This method is divided into three main steps. The first step is generating the print path. The second step is optimizing the print path in real time. The final step is integrating this method into the print control system.





### 3.3.1 3D printing path generation

By combining the potential field (Hwang & Ahuja, 1992) method and motion planning based on the sampling method (Lindemann & LaValle, 1992), in conjunction with the framework of the 3D reconstruction algorithm, a path through the complex environment on the lunar surface that avoids obstacles in real time can be generated to safely move the mobile carrier to the lunar base construction site. The global origin coordinates of the building is determined, and the mobile carrier's construction path is generated using the shortest path algorithm and real-time lunar scene sampling. After the mobile carrier reaches the target origin coordinate, the printing motion path of the robotic arm that corresponds to the pose of each mobile carrier is generated using a geometric algorithm; the mobile carrier autonomously perceives and recognizes environmental parameters and calculates the printing path in real time to avoid collisions.

### 3.3.2 Real-time 3D printing path optimization

Based on the existing printing path trajectories and the constraints of the robot's dynamics and speed kinematics, the path is optimized to improve the printing efficiency; an appropriate algorithm for path smoothing, such as splines, polynomial interpolation, Bezier curves, and Fourier series, is selected. Based on the real-time feedback of the robot arm joint sensor, structured light, and visual camera, the relative relationship between the geometric boundary of the printing object and the TCP calibration of the printing execution end is accurately identified; the printing path is optimized under different task constraints to achieve optimum parameters of accuracy, speed, pose angle and distance.

### 3.3.3 An integrated construction process

Achieving an integrated construction process on the lunar surface involves the development of a large-scale lunar regolith 3D printing system, a cross-scale environment sensing and feedback system, and a lunar soil 3D laser-printing lightweight tool end. The robotic arm's posture and printing path are derived in real time, and the printing tasks are automatically divided at each stage; multiscale information such as architectural geometric information, lunar field information, and construction information are studied and integrated to obtain a multistage coupling construction method.

## 4 Lunar base 3D laser-printing construction material and technology

To achieve the above vision, research on 3D laser-printing building materials and technologies for lunar bases is needed (Fig. 5). The required research steps include the following steps.

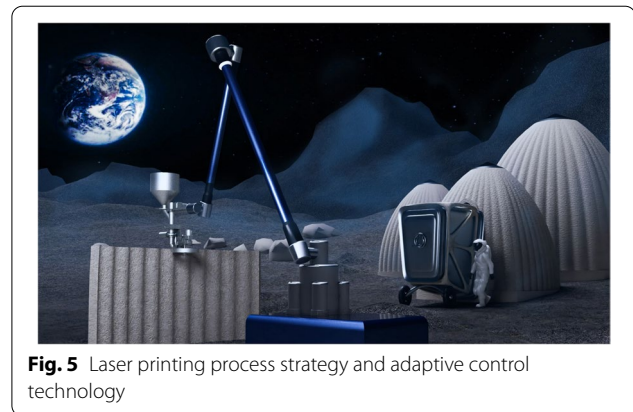


**Fig. 5** Laser printing process strategy and adaptive control technology

1. The law of interaction between the lunar soil-PAEK hybrid powder and the laser beam in the lunar surface environment is investigated, their interface bonding mechanism and influencing factors are analyzed, and the technical principle of mixed powder laser-printing technology is proposed. The energy diffusion behavior of the mixed powder is examined under the effect of different laser wavelengths, the impact of the PAEK mass ratio and particle size is evaluated, and the optimal matching scheme of the mixed powder and laser wavelength are determined.
2. The dual-light field coupling laser-printing technology is developed, the mapping relationship between the process parameters, temperature field characteristics, and structural properties is established, the efficiency of the mixed powder molding process is improved, a quality and shape monitoring system is developed, and a self-adaptive control benchmark system is established for parameters such as powder thickness, motion speed, and laser power.
3. The strategy for the whole process is optimized, including powder transportation, powder laying, powder printing and compaction, design and manufacture optimized wavelength lasers, beam-shaping components, and integrated actuators. Moreover, the integration of the lightweight tool end for 3D laser printing with lunar regolith is achieved.

### 4.1 Lunar regolith hybrid powder preparation and forming mechanism

This part of the section shows a focus on the research method of Lunar regolith material, which is divided into three parts (Fig. 6). First, the laser response behavior of lunar regolith and polyaryletherketone mixed powder is studied separately. Second, the optimal laser wavelength and powder ratio are discussed. Finally, the possible defects in laser printing are studied.

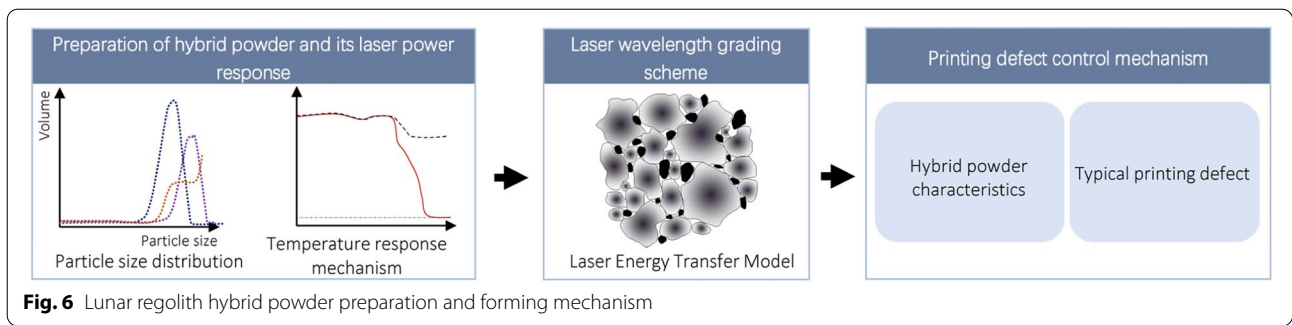


**Fig. 6** Lunar regolith hybrid powder preparation and forming mechanism

**4.1.1 Preparation of hybrid powder of lunar soil and polyaryletherketone and its laser reactivity**

Based on actual lunar regolith samples, hybrid powders simulating lunar regolith with the same composition ratio and particle size distribution should be created. PAEK is chosen as the printing binder due to its material strength, adhesion qualities, and extreme environmental adaptability. The melting temperature, glass transition temperature, viscosity, and other properties of PAEK should be optimized according to the actual printing environment on the lunar surface. Under the influence of several laser wavelengths, the heating law and the evolution of the physicochemical properties of the hybrid powder should be analyzed.

**4.1.2 Binding mechanism of hybrid powder and its gradation scheme with laser wavelength**

A thermodynamic model should be developed to examine the direction and rate of energy transfer within the hybrid powder. This model can reveal the interfacial bonding mechanism between lunar soil and PAEK and the effect of temperature field distribution on the interfacial bonding state. Moreover, the rate of energy diffusion is characterized along the thickness direction of the powder under the action of different wavelengths of laser. The particle size and weight ratio of PAEK are

optimized to help the hybrid powder achieve stable, mild and high penetrating absorption of laser energy. The distribution characteristics of lunar soil and PAEK after the laser thermal fusion process are revealed. In addition, the matching formula for hybrid powder and laser wavelength are obtained.

**4.1.3 Control of the defect formation in hybrid powder laser printing**

When the hybrid powder is heated by a laser to reach the melting temperature of PAEK, it forms an organic and inorganic interface bond. To control the defect formation in this hybrid powder printing, the mapping relationship between the interfacial bond strength, the porosity of the printed body, the burning behavior of PAEK, the internal stress and deformation, the time, and the temperature field of the printing area should be studied. The optimal interface bonding of the hybrid powder can be achieved by adjusting the strength of the laser beam energy.

**4.2 Laser printing process strategy and adaptive control technology**

In this section, the process and strategy of laser printing (Fig. 7) are presented. These process and strategy are divided into three main parts. First, the delivery method of hybrid powder is proposed. Second, the dual-light field coupling laser technology for printing is proposed.

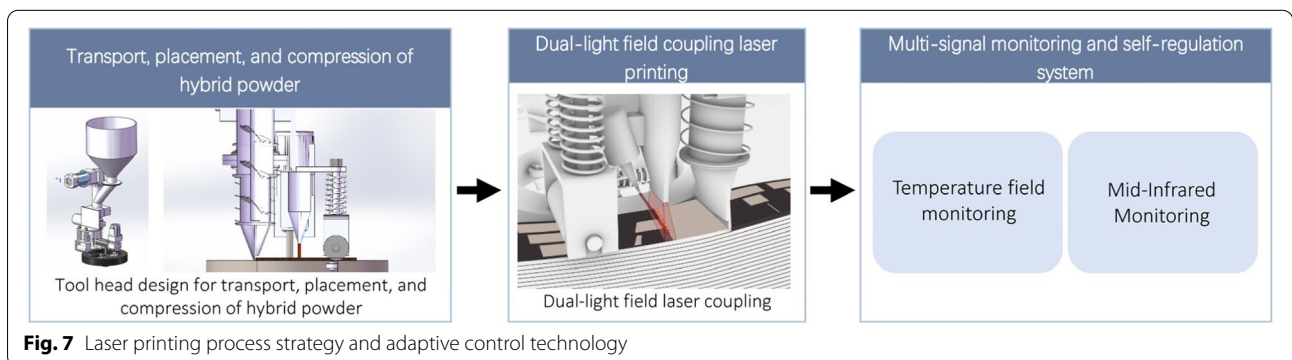


**Fig. 7** Laser printing process strategy and adaptive control technology

Finally, the real-time monitoring method of the printing process is proposed.

**4.2.1 Transport, placement, and compression of hybrid powder**

Due to the environmental characteristics of low gravity and vacuum atmospheric conditions on the lunar surface, the strategy of mechanical extrusion transportation is adopted to transport and lay the hybrid powder after screening and preparation. The mobile powder scraping device is designed to fit the shape of the lunar base wall to ensure that each layer of the printing powder is applied with uniform thickness. After the occurrence of the laser hot melt printing, conformal cooling rollers are utilized for compaction. The quantitative relationship between the thickness of the powder and the degree of compaction and the printing quality should be revealed, and the powder bond can be further strengthened by regulating the structure and downforce of the cooling rollers.

**4.2.2 Dual-light field coupling laser-printing technology research and optimization**

Using a dual-light field laser-printing strategy coupled with a low-power density large-size light spot and a high-power density small-size focused light spot, the dual-light field space and energy distribution are optimized to obtain a nearly uniform distribution of the temperature field in the printing area. In a larger printing area, the powder base temperature is increased and is then further heated to the preset printing temperature by focusing the light spot. The large light spot moves at the same speed in the direction of powder laying, while the focused light spot is scanned quickly in the large light spot area. This compound motion enables a high-efficiency printing and forming process. In addition, the effect of the scanning parameters such as the laser power and scanning speed on the temperature field is investigated, and a process database for a variable-section wall structure is developed.

**4.2.3 Multi-signal monitoring and regulation system**

A multi-signal monitoring and regulation system is required in a high complexity laser-printing process. To ensure printing quality, a real-time laser power control system is used to ensure that the temperature field in the printing area is relatively stable within the optimized process window; a structure and topography monitoring system based on structured light technology is established to monitor and regulate the relationship between the printing parameters and printing accuracy. The establishment of a 3D printing accuracy prediction model lays the foundation for high-precision closed-loop control of process parameters such as the powder coating thickness, laser power, and printing speed of the large-scale printing actuator on the lunar surface.

**4.3 Lightweight 3D laser-printing tool**

In this section, the design process of the lightweight printing device (Fig. 8) is described. This process is divided into three main parts. First, the design of the laser generator is developed. Second, the quality and shape monitoring system is studied. Finally, the integration of the entire laser print actuator is evaluated.

**4.3.1 Wavelength-specific lasers and beam-shaping instrument**

The MOPA structure thulium-doped fiber laser (Lv et al., 2012) technology is used to develop a specific wavelength fiber laser in the mid-infrared band and obtain a laser wavelength that corresponds to the formula of the mixed powder to ensure that the optimal bonding state of the mixed powder is achieved. The laser output beams were split. One beam was prepared with a DOE beam shaping element (Katz et al., 2018) to create a rectangular flat-top spot matching the size of the building wall, while the other beam was collimated, expanded, and focused. The preset multilight field coupled beam printing procedure is achieved through the optimal matching of the double light field space and energy.

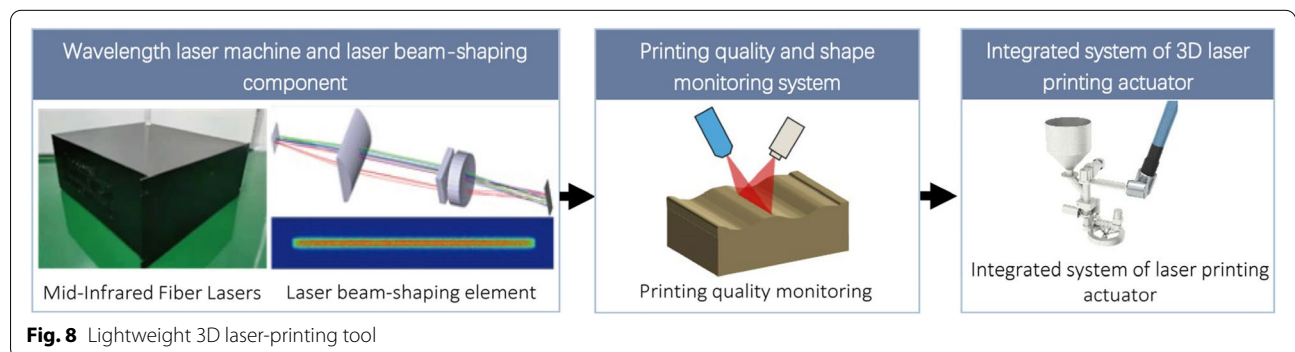


**Fig. 8** Lightweight 3D laser-printing tool

#### 4.3.2 Quality and shape monitoring system

The infrared temperature measurement system is used to monitor the printing area's temperature field in real time. Feedback signals from the system are transferred to the laser control system to help regulate the strength of the laser beam energy. A laser structured light profiler-based sensor is built to rapidly detect and obtain the quality and shape characteristics of the printed structure. The local topography rapid splicing and imaging technology are researched. Finally, a characterization method for the key variables of the overall accuracy of the printing process is proposed.

#### 4.3.3 Integrated laser-printing actuator

Based on the optimized process strategy of mixing powder conveying, laying, printing, and compacting, a laser-printing actuator with the characteristics of compact size, large processing area, and light weight was developed. The Z-direction additional axis is set for the height compensation of the printing actuator to ensure constant squeegee thickness and laser focus position, to optimize the relative relationship between the spatial positions of each process, to ensure the printing quality and topographic accuracy and to match the printing rhythm of each process for enhancing the printing efficiency.

## 5 Experiments

In this experiment, a mid-infrared laser was used to sinter the hybrid powder of synthetic lunar regolith and PAEK. To demonstrate the feasibility and effectiveness of this method, the author conducted relevant preliminary experiments, including testing the wavelength of the laser, the temperature range of sintering, the proportion of hybrid powder, and the compaction rate.

#### 5.1 Optimal temperature range for hybrid powder printing

JSC-1A is the synthetic lunar regolith used in this experiment. The synthetic lunar regolith is prepared with reference to the components of Lunar soil 14,163 (Li et al., 2019a, 2019b). Its primary constituents are simple oxides, with  $\text{SiO}_2$  constituting the highest fraction, followed by  $\text{Al}_2\text{O}_3$ ,  $\text{CaO}$ ,  $\text{FeO}$ , and other elements. Previous research has demonstrated that these powders have a high laser light absorption rate (Li et al., 2019a, 2019b).

We conducted an experiment to examine the response of PAEK to different laser wavelengths. FT-IR spectra were recorded on a German BRUKER TENSOR II spectrometer with a resolution of  $4\text{ cm}^{-1}$ , and 32 scans were available for an acceptable signal-to-noise ratio. The scanning sampling range was  $550$  to  $4000\text{ cm}^{-1}$ . In the experiment, it was determined that the resin powder had a low absorption rate for light with a wavelength of  $2\text{ }\mu\text{m}$  (Fig. 9), and at the same time, the lunar soil powder

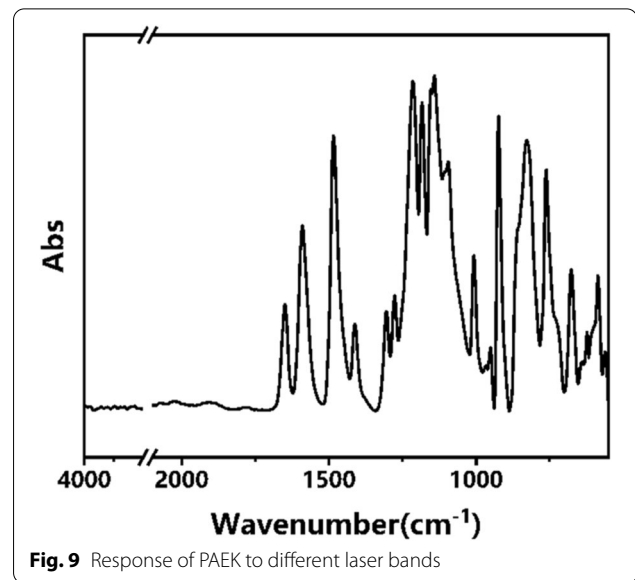


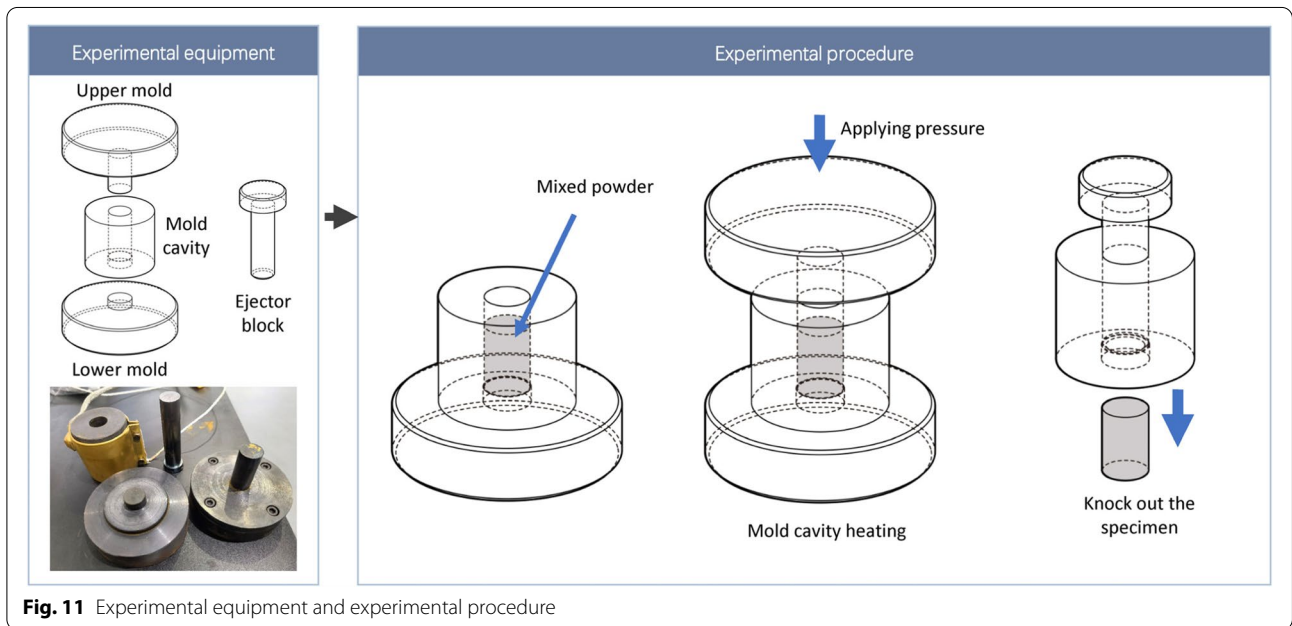
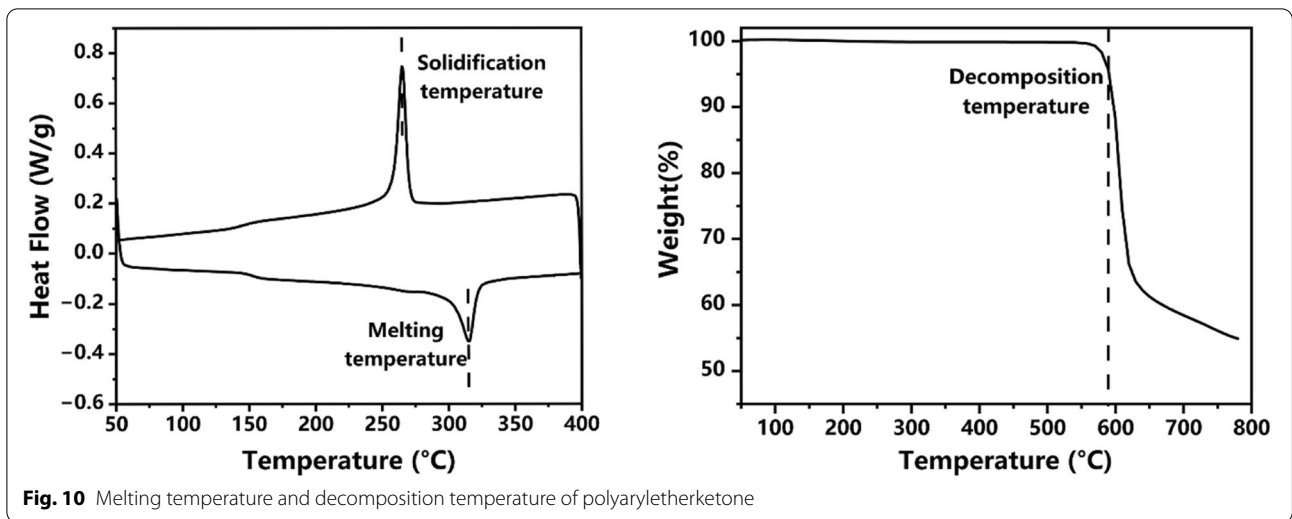
Fig. 9 Response of PAEK to different laser bands

had a high absorption rate for light with a wavelength of  $2\text{ }\mu\text{m}$  (Li et al., 2019a, 2019b). In aerospace applications, the  $2\text{-}\mu\text{m}$  laser band is relatively mature and broadly used due to its high stability. The author chose a  $2\text{ }\mu\text{m}$  wavelength to sinter the hybrid powder. In the hybrid powder, the proportion of lunar regolith is much higher than that of PAEK, which will form a clear energy transfer route from lunar soil to PAEK throughout the printing process to heat PAEK uniformly and gently and assure a satisfactory sintering effect.

The most important component in ensuring print quality is determining the optimal temperature range for hybrid powder.

Two experiments were conducted to determine the decomposition temperature and melting temperature of polyaryletherketone. The former used a TGA550 heat loss analyzer, the test temperature range was  $50\text{ }^\circ\text{C}$ - $800\text{ }^\circ\text{C}$ , the test gas was nitrogen, and the temperature rise rate was selected as  $10\text{ }^\circ\text{C}/\text{min}$ . The latter used a TA DSC 250 instrument from the USA. The test interval of the specimen was  $50\text{ }^\circ\text{C}$ - $400\text{ }^\circ\text{C}$ , the nitrogen flow rate was  $50\text{ ml}/\text{min}$ , and three scans were performed. The temperature was first increased, then decreased, and then increased, and the temperature rise rate was  $10\text{ }^\circ\text{C}/\text{min}$ . It was found that the hybrid powder started to melt at  $310\text{ }^\circ\text{C}$  and decomposed at  $510\text{ }^\circ\text{C}$  (Fig. 10). During the printing process, the heating gradient, temperature forming space, cooling gradient, and printing time are plotted on a chart for observation. From the chart, it is obvious that the printing temperature should be maintained between  $360$  and  $450\text{ }^\circ\text{C}$ . Time management is a crucial aspect of a high-quality bonding interface. A large light spot is used to warm the mixed powder, while a small





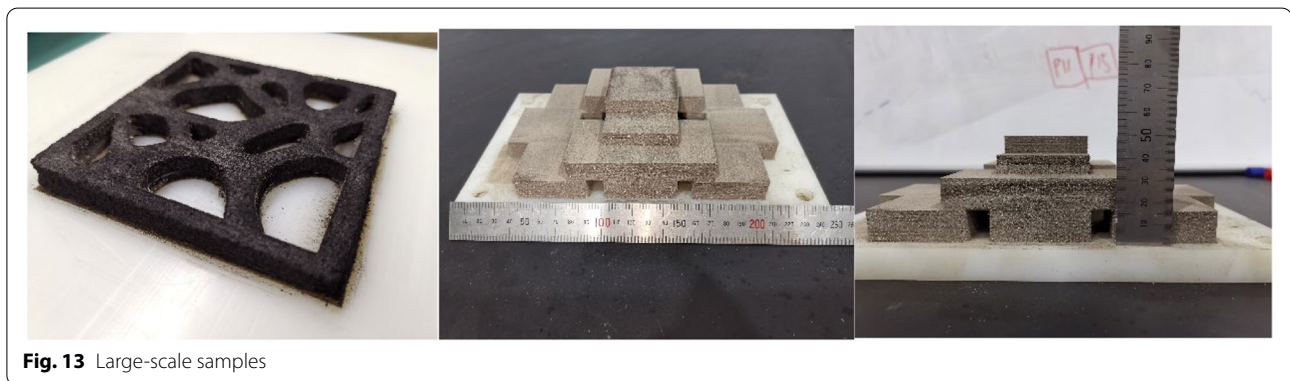
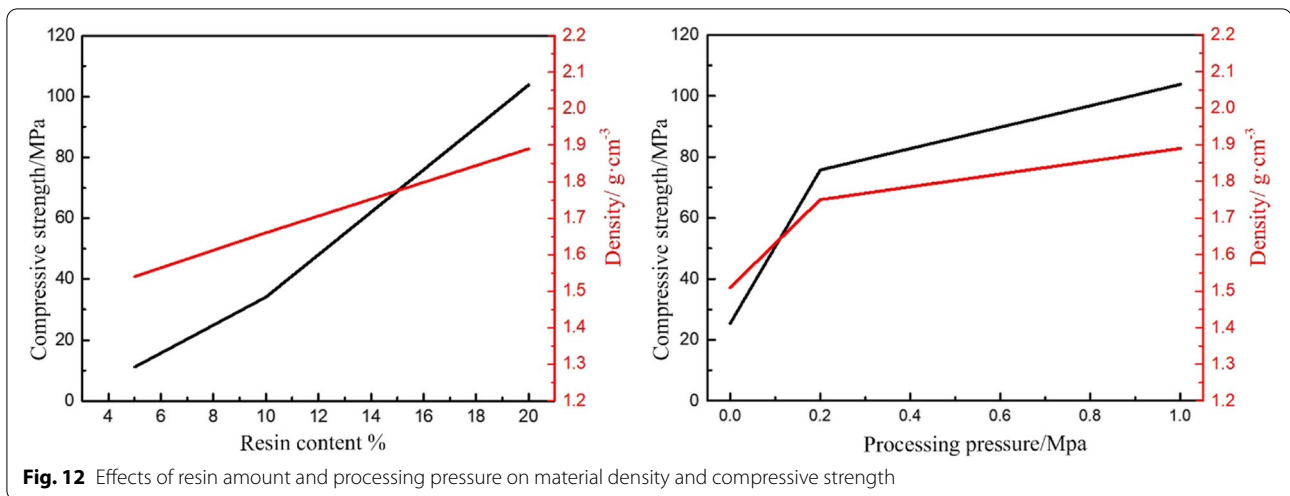
light spot is simultaneously used to achieve sintering at a specific location.

### 5.2 The ratio of lunar soil-PAEK and the rate of soil compaction

The ratio of resin to lunar soil and the compaction rate are two important factors that influence the performance of hybrid lunar soil powder after printing.

In our experiments (Fig. 11), the thermoforming methodology was used to examine the effect of the resin amount and processing pressure on the compressive strength of the sintered samples. The experimental mold consists

of an upper mold, lower mold, mold cavity and ejector block, and the size of the sample is  $\phi 20 \text{ mm} \times 20 \text{ mm}$  ( $\pm 2 \text{ mm}$ ). In the experiment, the resin fine powder that is formulated into moon soil is first stirred well and added into the installed lower mold and mold cavity. In addition, the upper mold will be added into the mold cavity, adding weights on the upper mold until the pressure at the specimen stress area reaches the sample making requirements. Then, the mold cavity heating set is energized, the temperature is set to  $370^\circ\text{C}$ , and the temperature reaches the requirement after holding heat for 40 minutes. Finally, the mold cavity heating is closed, and the mold and specimen



need to be cooled down to the resin glass transition temperature below. The upper mold and lower mold were removed, the ejector block was placed into the mold cavity, and the specimen was knocked. The hot-pressing temperature in the experiment was controlled at 370°C, and the processing time was controlled at 40 minutes. The experimental results (Fig. 12) show that the compressive strength of the sample increases gradually when the resin content increases from 4% to 20%. When the processing pressure was increased from 5 MPa to 20 MPa, the sample's compressive strength steadily increased, but its growth rate gradually decreased. Taking into account the cost-effectiveness of earth-moon material transport and the viability and dependability of the lunar surface environment, a hybrid powder with a 20% resin content was preliminarily selected as the raw building material for 3D printing on the lunar surface based on the results of a hot-pressing experiment. In addition, the experiment also demonstrated that the compaction rate has a significant impact on the performance of 3D printing; thus, tapping and compacting must be performed after powder distribution.

### 5.3 Large-scale sample experiments - horizontal and vertical directions

Using the above parameters for the hybrid powder ratio and laser power, two lunar soil samples on a decimeter scale were produced in this study (Fig. 13). These two samples verified the feasibility of the laser powder bed printing process in both horizontal and vertical dimensions. The first is a sectional sample of the wall's interior. The printing results demonstrate that selective laser fusion printing on the hollow structure can ensure uniform stress on the structure. The second sample examined the feasibility of printing a complex shape in the vertical direction and successfully printed a three-layer cross-dislocation structure.

## 6 Conclusion

The construction and design of a lunar base is a new topic of discussion in the current architectural design theory study. From the discussion above, this study draws the following conclusions.



**Fig. 14** Lunar surface base and lunar surface robot

- Due to the high cost of transportation from Earth to the lunar surface and considering the complexity and variability of the lunar environment, it is concluded that among the three phases of lunar base construction in history, in situ construction is the most cost-effective and has the greatest development potential due to its comprehensive utilization of in situ lunar resources.
- When constructing a lunar base, the rationality and constructability of the lunar base scheme must be considered. In this case, the use of 3D printing technology is the most flexible and adaptable.
- Since in situ construction is largely dependent on environmental and lunar surface solutions, it is vital to develop a comprehensive process system that can adapt to a variety of challenging scenarios.

In this study, a prototype for a lunar base concept (Fig. 14) is proposed to support astronaut life and scientific research on the moon. With the intention of creating a lightweight, reconfigurable, and structural performance-based in situ construction lunar base, the physical mapping relationship between the extreme environment of the lunar surface and the design properties of the lunar building structure are studied in this paper. At the same time, the principle of a high-performance bionic structure is investigated and applied to the design of the prototype of the lunar base. In terms of materials, the interfacial bonding mechanism of hybrid powder was investigated to study the best ratio for lunar regolith and PAEK. Finally, the optimal wavelength laser and integrated actuator are designed and produced to complete the development of the lightweight lunar soil laser-printing tool end.

Conceptually, the technology presented in this study avoids many of the anticipated issues with in situ 3D printing of lunar bases, but for actual lunar base construction, many surprises and unknowns remain. A lunar base building can fail due to equipment problems caused by lunar

dust, radiation, harsh temperatures, printing errors due to topographic terrain, etc. To address these difficulties, future research on concepts such as self-healing robots must be further explored. In addition, the coupled construction experiment of the lunar environment requires special equipment and test conditions. At this stage, there is no existing dedicated laboratory that supports the simulation of the lunar base's construction on the lunar surface.

In this study, a concept for a lunar outpost from the standpoint of intelligent building design is proposed. This concept requires significant contributions from other domains. As a case study of a lunar base building, this plan is distinctive in its responsive design and unique construction approach, setting it apart from other schemes in the research literature. The design details presented in this paper can serve as a reliable sample for future lunar base construction research.

#### Acknowledgements

Not applicable.

#### Authors' contributions

The author(s) read and approved the final manuscript.

#### Funding

National Science Foundation of China-Shenzhen Joint Fund (CN), No. U1913606.

Science and Technology Innovation Plan of Shanghai Science and Technology Commission, No. 21DZ1204500.

#### Availability of data and materials

Not applicable.

#### Declarations

#### Competing interests

The authors declare that they have no known competing financial interests or personal relationships that could have appeared to influence the work reported in this paper.

Author Philip F. YUAN is a member of the Editorial Board for *Architectural Intelligence* and was not involved in the journal's review of or decisions related to this manuscript.

#### Author details

<sup>1</sup>College of Architecture and Urban Planning, Tongji University, Shanghai, China. <sup>2</sup>Shanghai Aerospace Equipments Manufacturer Co., Ltd, Shanghai, China. <sup>3</sup>Shanghai Institute of Optics and Fine Mechanics, Chinese Academy of Sciences, Shanghai, China. <sup>4</sup>Center for Advanced Low-dimension Materials, Donghua University, Shanghai, China.

Received: 5 June 2022 Accepted: 29 August 2022

Published online: 27 September 2022

#### References

- Allende, M. I., Miller, J. E., Davis, B. A., Christiansen, E. L., Lepech, M. D., & Loftus, D. J. (2020). Prediction of micrometeoroid damage to lunar construction materials using numerical modeling of hypervelocity impact events. *International Journal of Impact Engineering*, 138, 103499.
- Anand, M., Crawford, I. A., Balat-Pichelin, M., Abanades, S., Van Westrenen, W., Péraudeau, G., et al. (2012). A brief review of chemical and mineralogical resources on the moon and likely initial in situ resource utilization (ISRU) applications. *Planetary and Space Science*, 74(1), 42–48.

- Avelino, R. M., Iannuzzo, A., Van Mele, T., & Block, P. (2021). Assessing the safety of vaulted masonry structures using thrust network analysis. *Computers & Structures*, 257, 106647.
- Balla, V. K., Roberson, L. B., O'Connor, G. W., Trigwell, S., Bose, S., & Bandyopadhyay, A. (2012). First demonstration on direct laser fabrication of lunar regolith parts. *Rapid Prototyping Journal*. <https://doi.org/10.1108/13552541211271992>
- Baum, M. C. (2006). Centennial challenges, millennium opportunities. *The American Journal of Occupational Therapy*, 60(6), 609.
- Ceccanti, F., Dini, E., De Kestelier, X., Colla, V., & Pambaguian, L. (2010). 3D printing technology for a moon outpost exploiting lunar soil. In *Proceeding of the 61st international Astronautical congress IAC* (pp. 1–9).
- Cesaretti, G., Dini, E., De Kestelier, X., Colla, V., & Pambaguian, L. (2014). Building components for an outpost on the lunar soil by means of a novel 3D printing technology. *Acta Astronautica*, 93, 430–450. <https://doi.org/10.1016/j.actaastro.2013.07.034>
- Chen, Z., Li, Z., Li, J., Liu, C., Lao, C., Fu, Y., et al. (2019). 3D printing of ceramics: A review. *Journal of the European Ceramic Society*, 39(4), 661–687. <https://doi.org/10.1016/j.jeurceramsoc.2018.11.013>
- Dudley-Rowley, M., Gangale, T., Lemke, L., & Cohen, M. M. (2005). Habor lunar crew size, skill mix, and time model. *Margin*, 1, 0–4.
- Evans, M. E., & Graham, L. D. (2020). A flexible lunar architecture for exploration (FLARE) supporting NASA's Artemis program. *Acta Astronautica*, 177, 351–372. <https://doi.org/10.1016/j.actaastro.2020.07.032>
- Fateri, M., Gebhardt, A., Gabrielli, R. A., Herdich, G., Fasoulas, S., Großmann, A., et al. (2015). Additive manufacturing of lunar regolith for extra-terrestrial industry plant. In *Proc., 30th Int. Symp. on Space Technology and Science*.
- Fiske, M., & Edmunson, J. (2017). *Additive construction with mobile emplacement (ACME) 3D printing structures with in-situ resources (No. MSFC-E-DAA-TN48929)*.
- Foster + Partners. (2012). Lunar Habitation. [Fosterandpartners.com](https://www.fosterandpartners.com/projects/lunar-habitation/). Retrieved May 1, 2022, from <https://www.fosterandpartners.com/projects/lunar-habitation/>
- Gailiunas, P. (2015). *The evolution of shell lace structure, by Mike Tonkin and Anna Liu*.
- Goins, N. R., Dainty, A. M., & Toksöz, M. N. (1981). Lunar seismology: The internal structure of the moon. *Journal of Geophysical Research: Solid Earth*, 86(B6), 5061–5074.
- Goulas, A., Binner, J. G., Engström, D. S., Harris, R. A., & Friel, R. J. (2019). Mechanical behaviour of additively manufactured lunar regolith simulant components. *Proceedings of the Institution of Mechanical Engineers, Part L: Journal of Materials: Design and Applications*, 233(8), 1629–1644. <https://doi.org/10.1177/1464420718777932>
- Goulas, A., Binner, J. G., Harris, R. A., & Friel, R. J. (2017). Assessing extraterrestrial regolith material simulators for in-situ resource utilisation based 3D printing. *Applied Materials Today*, 6, 54–61. <https://doi.org/10.1016/j.apmt.2016.11.004>
- He, C., Zeng, X., & Wilkinson, A. (2013). Geotechnical properties of GRC-3 lunar simulant. *Journal of Aerospace Engineering*, 26(3), 528–534. [https://doi.org/10.1061/\(ASCE\)AS.1943-5525.0000162](https://doi.org/10.1061/(ASCE)AS.1943-5525.0000162)
- Hintze, P., Curran, J., & Back, T. (2009). Lunar surface stabilization via sintering or the use of heat cured polymers. In *47th AIAA Aerospace Sciences Meeting including The New Horizons Forum and Aerospace Exposition* (p. 1015). <https://doi.org/10.2514/6.2009-1015>
- Howe, A., & Gibson, I. (2006). MOBILAT2: A mobile habitat based on the trigon construction system. In *Space 2006* (p. 7337). <https://doi.org/10.2514/6.2006-7337>
- Howe, A. S., & Sherwood, B. (2009). *Out of this world: The new field of space architecture: The new field of space architecture*. American Institute of Aeronautics and Astronautics. <https://doi.org/10.2514/4.479878>
- Hwang, Y. K., & Ahuja, N. (1992). A potential field approach to path planning. *IEEE Transactions on Robotics and Automation*, 8(1), 23–32.
- Jakus, A. E., Koube, K. D., Geisendorfer, N. R., & Shah, R. N. (2017). Robust and elastic lunar and martian structures from 3D-printed regolith inks. *Scientific Reports*, 7(1), 1–8. <https://doi.org/10.1038/srep44931>
- Jiang, M., Li, L., & Sun, Y. (2012). Properties of TJ-1 lunar soil simulant. *Journal of Aerospace Engineering*, 25(3), 463–469. [https://doi.org/10.1061/\(ASCE\)AS.1943-5525.0000129](https://doi.org/10.1061/(ASCE)AS.1943-5525.0000129)
- Katz, S., Kaplan, N., & Grossinger, I. (2018). Using diffractive optical elements: DOEs for beam shaping—fundamentals and applications. *Optik & Photonik*, 13(4), 83–86.
- Kennedy, K., & Toups, L. (2008). Constellation Architecture Team-Lunar Habitation Concepts. In *AIAA SPACE 2008 Conference & Exposition* (p. 7633). <https://doi.org/10.2514/6.2008-7633>
- Khoshnevis, B., Bodiford, M., Burks, K., Ethridge, E., Tucker, D., Kim, W., et al. (2005). Lunar contour crafting—a novel technique for ISRU-based habitat development. In *43rd AIAA Aerospace Sciences Meeting and Exhibit* (p. 538). <https://doi.org/10.2514/6.2005-538>
- Khoshnevis, B., & Zhang, J. (2015). Selective separation sintering (SSS)—an additive manufacturing approach for fabrication of ceramic and metallic parts with application in planetary construction. In *AIAA SPACE 2015 Conference and Exposition* (p. 4450). <https://doi.org/10.2514/6.2015-4450>
- King, O., Warren, T., Bowles, N., Sefton-Nash, E., Fisackerly, R., & Trautner, R. (2020). The Oxford 3D thermophysical model with application to PROSPECT/Luna 27 study landing sites. *Planetary and Space Science*, 182, 104790. <https://doi.org/10.1016/j.pss.2019.104790>
- Knippers, J., Schmid, U., & Speck, T. (2019). *Biomimetics for architecture: Learning from nature*. Birkhäuser.
- Lee, T. S., Lee, J., & Ann, K. Y. (2015). Manufacture of polymeric concrete on the moon. *Acta Astronautica*, 114, 60–64. <https://doi.org/10.1016/j.actaastro.2015.04.004>
- Li, C., Wang, C., Wei, Y., & Lin, Y. (2019). China's present and future lunar exploration program. *Science*, 365(6450), 238–239. <https://doi.org/10.1126/science.aax9908>
- Li, H., & Englund, K. (2017). Recycling of carbon fiber-reinforced thermoplastic composite wastes from the aerospace industry. *Journal of Composite Materials*, 51(9), 1265–1273. <https://doi.org/10.1177/0021998316671796>
- Li, S., Lucey, P. G., Milliken, R. E., Hayne, P. O., Fisher, E., Williams, J. P., et al. (2018). Direct evidence of surface exposed water ice in the lunar polar regions. *Proceedings of the National Academy of Sciences*, 115(36), 8907–8912. <https://doi.org/10.1073/pnas.1802345115>
- Li, W., Xu, K., Huang, Y., Hu, W., Wang, D., & Yao, S. (2019). In-situ forming of lunar regolith simulant via selective laser melting. *Journal of Beijing University of Aeronautics and Astronautics*, 45(10), 1931.
- Lin, T. D., Senseney, J. A., Arp, L. D., & Lindbergh, C. (1989). Concrete lunar base investigation. *Journal of Aerospace Engineering*, 2(1), 10–19.
- Lindemann, S. R., & LaValle, S. M. (2005). Current issues in sampling-based motion planning. In *Robotics research. The eleventh international symposium* (pp. 36–54). Springer.
- Liu, M., Tang, W., Duan, W., Li, S., Dou, R., Wang, G., et al. (2019). Digital light processing of lunar regolith structures with high mechanical properties. *Ceramics International*, 45(5), 5829–5836. <https://doi.org/10.1016/j.ceramint.2018.12.049>
- Long, K., Yuan, P. F., Xu, S., & Xie, Y. M. (2018). Concurrent topological design of composite structures and materials containing multiple phases of distinct Poisson's ratios. *Engineering Optimization*, 50(4), 599–614.
- Lu, M., Zhu, W. R., & Yuan, P. F. (2020). Toward a collaborative robotic platform: FURBOT. In *Architectural intelligence* (pp. 87–101). Springer.
- Lv, H., Zhou, P., Xiao, H., Wang, X., & Jiang, Z. (2012). All-fiberized tm-doped fiber MOPA with 30-W output power. *Chinese Optics Letters*, 10(5), 051403.
- Magoffin, M., & Garvey, J. (1990). Lunar glass production using concentrated solar energy. In *Space Programs and Technologies Conference* (p. 3752). <https://doi.org/10.2514/6.1990-3752>
- McKay, D. S., Carter, J. L., Boles, W. W., Allen, C. C., & Allton, J. H. (1993). JSC-1: A new lunar regolith simulant. In *Lunar and Planetary Science Conference (Vol. 24)*.
- Mueller, R. P., Sibille, L., Hintze, P. E., Lippitt, T. C., Mantovani, J. G., Nugent, M. W., & Townsend, I. I. (2014a). Additive construction using basalt regolith fines. In *ASCE International Conference on Engineering, Science, Construction and Operations in Challenging Environments (No. KSC-E-DAA-TN17211)*.
- Mueller, R. P., Sibille, L., Hintze, P. E., Lippitt, T. C., Mantovani, J. G., Nugent, M. W., & Townsend, I. I. (2014b). Additive construction using basalt regolith fines. In *Earth and Space 2014* (pp. 394–403). <https://doi.org/10.1061/9780784479179.042>
- Nakamura, T., Van Pelt, A. D., Gustafson, R. J., & Clark, L. (2008). Solar thermal power system for oxygen production from lunar regolith. In *AIP conference proceedings (Vol. 969, no. 1, pp. 178-185)*. American Institute of Physics. <https://doi.org/10.1063/1.2844965>
- Oh, K., Chen, T., Kou, R., Yi, H., & Qiao, Y. (2020). Ultralow-binder-content thermoplastic composites based on lunar soil simulant. *Advances in Space Research*, 66(9), 2245–2250. <https://doi.org/10.1016/j.asr.2020.07.041>



- Rey-Rey, J. (2022). Nature as a source of inspiration for the structure of the Sydney opera house. *Biomimetics*, 7(1), 24.
- Rinaldi, M., Ferrara, M., Pigliaru, L., Allegranza, C., & Nanni, F. (2021). Additive manufacturing of polyether ether ketone-based composites for space application: A mini-review. *CEAS Space Journal*, 1–11. <https://doi.org/10.1007/s12567-021-00401-4>
- Sun, J., & Bhushan, B. (2012). Hierarchical structure and mechanical properties of nacre: A review. *RSC Advances*, 2(20), 7617–7632.
- Taylor, L. A., & Meek, T. T. (2005). Microwave sintering of lunar soil: Properties, theory, and practice. *Journal of Aerospace Engineering*, 18(3), 188–196. [https://doi.org/10.1061/\(ASCE\)0893-1321\(2005\)18:3\(188\)](https://doi.org/10.1061/(ASCE)0893-1321(2005)18:3(188))
- Taylor, S. L., Jakus, A. E., Koube, K. D., Ibeh, A. J., Geisendorfer, N. R., Shah, R. N., & Dunand, D. C. (2018). Sintering of micro-trusses created by extrusion-3D-printing of lunar regolith inks. *Acta Astronautica*, 143, 1–8. <https://doi.org/10.1016/j.actaastro.2017.11.005>
- Tomas, R., Katarina, E. & Ondrej, D. (2012). SINTERHAB. [Spacearchitect.org](http://Spacearchitect.org). Retrieved May 1, 2022, from <https://spacearchitect.org/portfolio-item/global-moon-village-2/>
- Travitzky, N., Bonet, A., Dermeik, B., Fey, T., Filbert-Demut, I., Schlier, L., et al. (2014). Additive manufacturing of ceramic-based materials. *Advanced Engineering Materials*, 16(6), 729–754. <https://doi.org/10.1002/adem.201400097>
- Vaniman, D., Reedy, R., Heiken, G., Olhoeft, G., & Mendell, W. (1991). *The lunar environment. The Lunar Sourcebook, CUP* (pp. 27–60).
- Williams, J. P., Paige, D. A., Greenhagen, B. T., & Sefton-Nash, E. (2017). The global surface temperatures of the moon as measured by the diviner lunar radiometer experiment. *Icarus*, 283, 300–325.
- Yuan, P. F., Song, Y., Lin, Y., Beh, H. S., Chao, Y., Xiao, T., et al. (2021). An architectural building cluster morphology generation method to perceive, derive, and form based on cyborg-physical wind tunnel (CPWT). *Building and Environment*, 203, 108045.
- Zhang, S., Wimmer-Schweingruber, R. F., Yu, J., Wang, C., Fu, Q., Zou, Y., et al. (2020). First measurements of the radiation dose on the lunar surface. *Science Advances*, 6(39), eaaz1334.
- Zhou, C., Chen, R., Xu, J., Ding, L., Luo, H., Fan, J., et al. (2019). In-situ construction method for lunar habitation: Chinese super Mason. *Automation in Construction*, 104, 66–79. <https://doi.org/10.1016/j.autcon.2019.03.024>

## Publisher's Note

Springer Nature remains neutral with regard to jurisdictional claims in published maps and institutional affiliations.